Nuclear structure of ^{229}Th

E. Ruchowska,[1,*] W. A. Płóciennik,[1,†] J. Żylicz,[2] H. Mach,[3] J. Kvasil,[4] A. Algora,[5] N. Amzal,[6] T. Bäck,[7] M. G. Borge,[8] R. Boutami,[8] P. A. Butler,[6] J. Cederkäll,[9] B. Cederwall,[7] B. Fogelberg,[3] L. M. Fraile,[9,‡] H. O. U. Fynbo,[9] E. Hagebø,[10] P. Hoff,[10] H. Gausemel,[10] A. Jungclaus,[8] R. Kaczarowski,[1] A. Kerek,[7] W. Kurcewicz,[2] K. Lagergren,[7] E. Nacher,[5] B. Rubio,[5] A. Syntfeld,[1] O. Tengblad,[8] A. A. Wasilewski,[1] and L. Weissman[9]

[1]*The Andrzej Sołtan Institute for Nuclear Studies, PL 05-400 Świerk, Poland*

[2]*Institute of Experimental Physics, University of Warsaw, PL 00-681 Warsaw, Poland*

[3]*Department of Radiation Sciences, University of Uppsala, SE-751 21 Uppsala, Sweden*

[4]*Department of Nuclear Physics, Charles University, CZ-18000 Prague 8, Czech Republic*

[5]*Instituto de Fízica Corpuscular, CSIC-University Valencia, E-46100 Burjassot, Spain*

[6]*Oliver Lodge Laboratory, University of Liverpool, Liverpool L69 3BX, United Kingdom*

[7]*Physics Department, Royal Institute of Technology, SE-106 91 Stockholm, Sweden*

[8]*Instituto de Estructura de la Materia, CSIC, E-28006 Madrid, Spain*

[9]*ISOLDE, CERN, CH-1211 Geneva 23, Switzerland*

[10]*Department of Chemistry, University of Oslo, Post Office Box 1033 Blindern, N-0315 Oslo, Norway*

(Received 28 December 2005; published 26 April 2006)

Lifetimes of excited states in ^{229}Th, populated in the β decay of ^{229}Ac, have been measured using the advanced time-delayed $\beta\gamma\gamma$(t) method. Half-lives of 14 states have been determined including 11 of them for the first time. Twenty-seven new γ lines have been introduced into the β-decay scheme of ^{229}Ac based on results of $\gamma\gamma$ coincidence measurements. Reduced transition probabilities have been determined for more than 70 γ transitions in ^{229}Th. Average $|D_0|$ values of 0.029(1), 0.077(3), and 0.024(5) e fm have been deduced for the lowest $K^\pi = 1/2^\pm$, $3/2^\pm$, and $5/2^\pm$ parity partner bands, respectively. Excited states in ^{229}Th and experimental transition rates have been interpreted within the quasiparticle-plus-phonon model. The half-life of the 3.5-eV, $3/2^+$ isomeric state is predicted to be about 10 h. Potential energy surfaces on the (β_2, β_3) plane for the lowest single quasiparticle configurations in ^{229}Th have been calculated using the Strutinsky method.

DOI: 10.1103/PhysRevC.73.044326 PACS number(s): 21.10.Tg, 21.10.Re, 21.10.Ky, 27.90.+b

I. INTRODUCTION

Spectroscopic studies of the ^{229}Th nucleus are very important for at least two reasons. First, ^{229}Th lies at the perimeter of the octupole deformation region in the actinides and the coexistence of reflection-symmetric and reflection-asymmetric shapes is expected in this nucleus [1]. Second, the first excited state in ^{229}Th at an energy of only 3.5(10) eV [2] is the lowest excited state known in all nuclei and the only one with excitation energy within the atomic energy scale (with recent evaluation [3] giving an energy of 5.5(10) eV for this state). Consequently, the lowest excited state in ^{229}Th presents a unique opportunity to investigate interactions between nuclear and atomic degrees of freedom and has been the main subject of several works in the past few years (e.g. [4–7] and references quoted therein). Although a direct observation of this state has not yet been possible, an estimate of its properties can be obtained by extrapolation from properties of the higher lying levels in ^{229}Th.

Excited states in ^{229}Th have been previously studied in the α decay of ^{233}U [8,9], β decay of ^{229}Ac [10], and electron-capture decay of ^{229}Pa [11] as well as in transfer reactions [12,13] and Coulomb excitations [14]. Recently, new studies on the β decay of ^{229}Ac [15] and on the α decay of ^{233}U [16] have been reported. Multipolarities of many γ transitions in ^{229}Th have been established in Ref. [15] by internal-conversion electron measurements. Lifetimes of the 42.3- and 97.1-keV levels have been measured in Ref. [17] and of the 146.4- and 164.5-keV levels in Ref. [15]. Despite a large body of experimental data on ^{229}Th only the structure of levels below 300 keV is clearly understood. To obtain a better understanding of the low-energy structure of ^{229}Th we have measured lifetimes of the excited states in this nucleus using the advanced time-delayed $\beta\gamma\gamma(t)$ method [18–20]. The experimental methods are briefly described in Sec. II, and the new level scheme for ^{229}Th and the lifetime results are presented in Sec. III of this paper. In Sec. IV experimental results are discussed in terms of the quasiparticle-plus-phonon model. Additionally, results of potential energy calculations on the (β_2, β_3) plane are also presented.

II. EXPERIMENTAL DETAILS

Measurements were carried out at the High Resolution Mass Separator (HRS) at the ISOLDE facility at CERN. Excited states in ^{229}Th were populated in the β decay of ^{229}Ac, which was obtained via a chain of β decays starting from the ^{229}Fr isotope:

$$^{229}\mathrm{Fr} \xrightarrow{50\,\mathrm{s}} {}^{229}\mathrm{Ra} \xrightarrow{4.0\ \mathrm{min}} {}^{229}\mathrm{Ac} \xrightarrow{62.7\ \mathrm{min}} {}^{229}\mathrm{Th}.$$

*Electronic address: ewa@ipj.gov.pl

†Deceased.

‡On leave from Universidad Complutense, E-28040 Madrid, Spain.

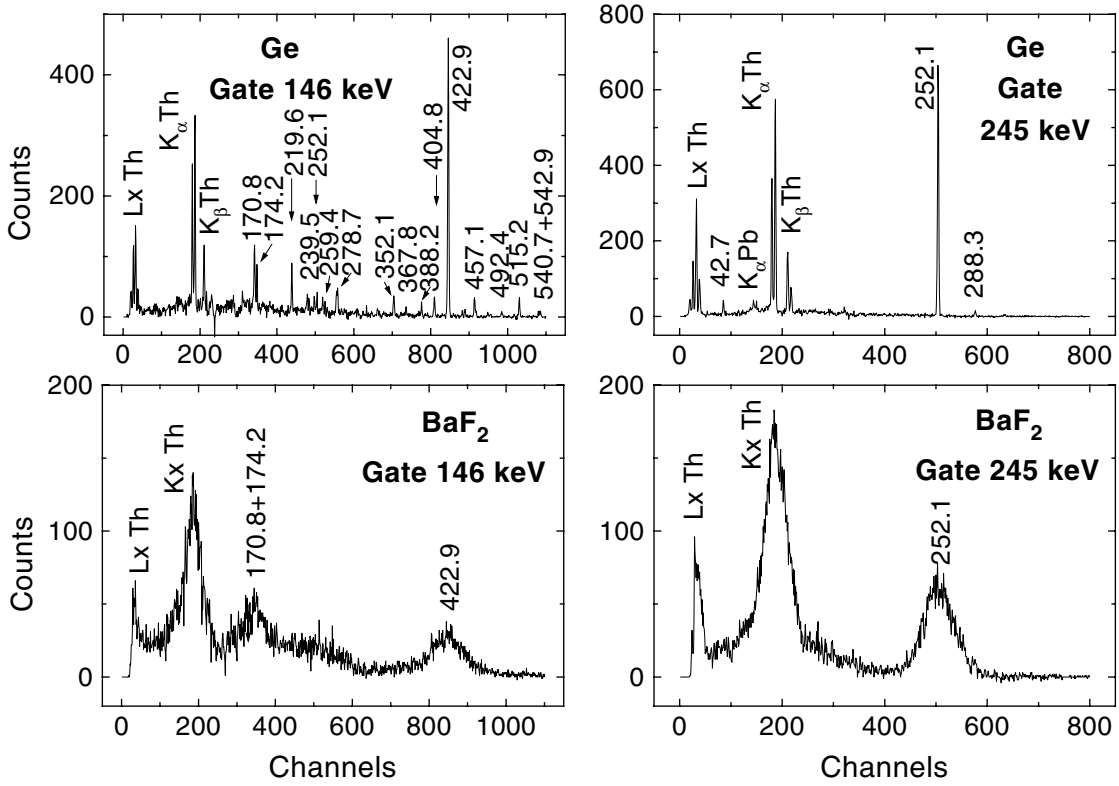

FIG. 1. Top panels show coincident γ-ray Ge spectra sorted from the β-Ge-Ge data using gates set on the 146.3- and 245.3-keV transitions. Panels at the bottom show the corresponding coincident γ-ray spectra sorted onto the BaF_2 detector using the β-Ge-BaF_2 data.

The ^{229}Fr nuclei were produced in the spallation reaction of ^{238}U induced by the 1.4-GeV protons from the Proton Synchrotron (PS) booster. The ^{229}Fr activity, mass separated from other spallation reaction products, was implanted onto an aluminium foil. After about 40 min of irradiation and 30 min of cooling time, the foil with almost pure activity of ^{229}Ac was placed in the center of our experimental setup.

Level lifetimes in the subnanosecond range have been measured with the advanced time-delayed $\beta\gamma\gamma$(t) method [18–20]. Fast timing information was derived from time-delayed coincidences between fast-response β and BaF_2 γ detectors, and additional coincidences with a Ge γ detector were used to select the desired γ cascade. A 3-mm-thick plastic scintillator NE111A was used as a β detector to ensure a constant time response independent of the energy of incident β particles. The setup consisted of two BaF_2 detectors in the shape of truncated cones with a height of 2.5 cm each and two HPGe detectors with efficiencies of about 40% and 70%, respectively. This resulted in one combination of β-Ge-Ge coincidences, which served to construct the level scheme, and four combinations of β-Ge-BaF_2 coincidences, which provided lifetime information. Triple- and higher-fold coincident events were collected and then presorted off-line into data sets with the triple coincidences already mentioned. Two independent series of measurements were performed, in which about 3.7×10^6 and 8.4×10^6 triple coincidence events were collected, respectively.

III. EXPERIMENTAL RESULTS

A. Level scheme

The results for ^{229}Th are presented in Figs. 1–4 and in Table I. The level scheme was constructed based on the β-Ge-Ge data. Examples of coincident γ-ray spectra collected with the Ge detectors are shown in the upper panels of Figs. 1–3; the new level scheme for ^{229}Th is presented in Figs. 4(a)–4(c). Level and γ-ray energies determined in the present work are given in columns 1 and 4 of Table I, respectively, and also in the level scheme. For several γ lines precise γ-ray energies were adopted from Ref. [2]. Some of these energies were used for internal energy calibration, which served to determine the energies of other lines in ^{229}Th. Where available, γ-ray intensities as well as $E2/M1$ mixing ratios were taken from Ref. [15]. (The intensity relations in our data have been distorted by the low-energy cutoff in the gating β signals.)

In general our level scheme for ^{229}Th agrees well with the one obtained by Gulda *et al.* [15]. The exception is the 526.75-keV level, for which no evidence was found in our data. Twenty-seven new γ lines have been introduced into the decay scheme of ^{229}Ac connecting levels already established in previous works. Six of them have already been observed in the α decay of ^{233}U [16]. New lines are marked by stars in Figs. 4(a)–4(c) and in Table I. Information on new transitions not listed in Table I is given in Table II. Highly converted transitions, which have not been directly observed

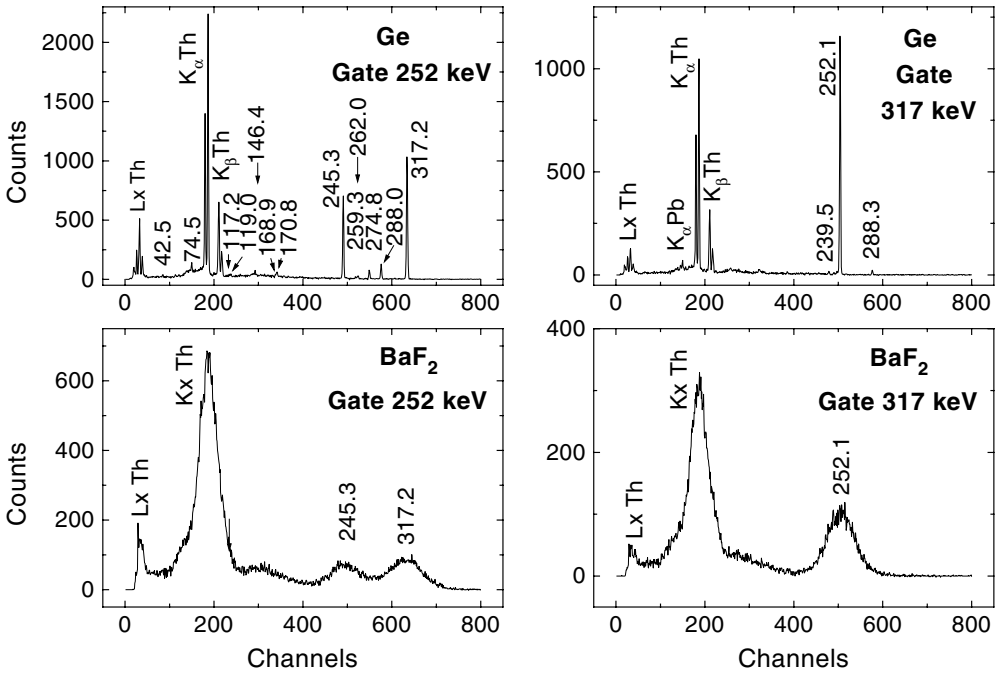

FIG. 2. Similar to Fig. 1 but gated on the 252.1- and 317.2-keV transitions.

in our spectra but whose existence has been established from our coincidence data, are drawn with dashed lines in the level scheme and are given in parentheses in Table I. For completeness, transitions seen by Gulda *et al*. [15], but not observed in our data because of the lower efficiency of our setup in the very low and high-energy ranges or because of restrictive coincidence requirements, are shown in the level scheme by dotted lines.

B. Level lifetimes

Level lifetimes were determined from the analysis of the triple coincidence β-Ge-BaF_2 data. The key to the analysis is a clean separation of the full energy peaks in the gating spectra. Examples of γ-ray BaF_2 spectra coincident to the gating transitions selected in the Ge detector are shown in the lower panels of Figs. 1–3.

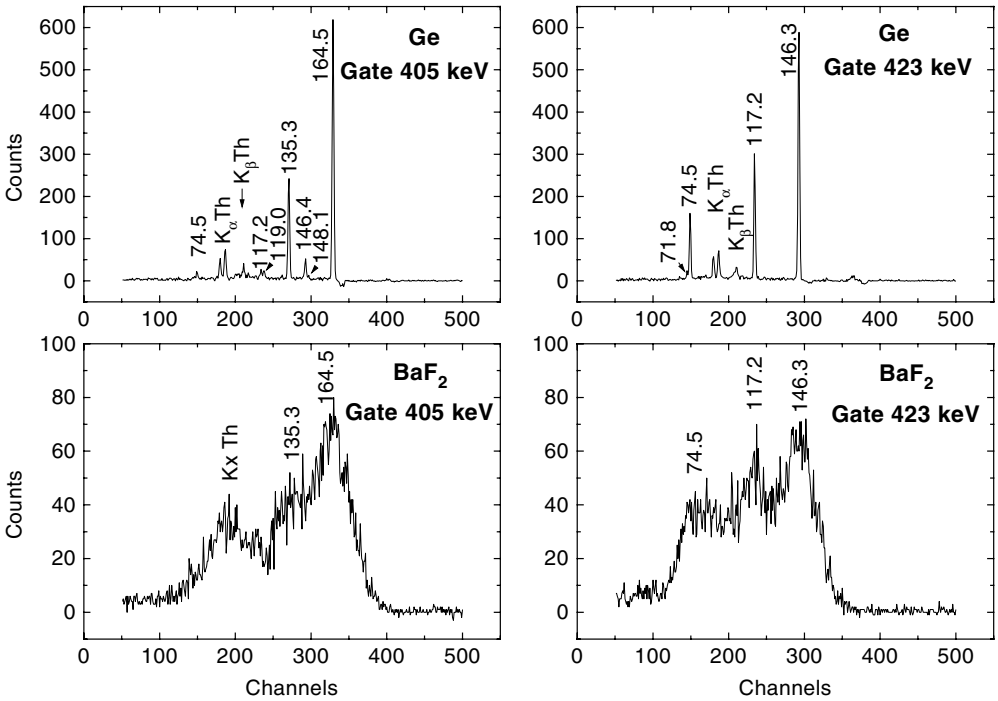

FIG. 3. Similar to Fig. 1 but gated on the 404.8- and 422.9-keV transitions.

TABLE I. Level lifetimes and experimental and theoretical reduced transition probabilities in ^{229}Th; γ-ray energies are determined in this work unless noted otherwise. New γ lines are marked by stars.

Initial level (keV)	$I_i K_i^\pi$	$T_{1/2}$ (ps)	E_γ (keV)	I_γ[a]	$I_f K_f^\pi$	$X\lambda$[a]	α_{TOT}[b]	$B_{\mathrm{exp}}(X\lambda)$[c]	$B_{\mathrm{theor}}(X\lambda)$
0.0035	3/2 3/2$^+$		(0.0035)		5/2 5/2$^+$	$M1$			2.5×10^{-2}
						$E2$			5.6×10^{3}
29.18	5/2 3/2$^+$		29.1846(30)[d]	1.98(8)	3/2 3/2$^+$	$M1$			1.1×10^{-2}
						$E2$			1.9×10^{4}
			(29.18)		5/2 5/2$^+$	$M1$			0.9×10^{-2}
						$E2$			4.1×10^{3}
42.34	7/2 5/2$^+$	172(6)[e]	42.34(10)	0.44(9)[f]	5/2 5/2$^+$	$M1$[g]	48.0	$1.8(5) \times 10^{-2}$	1.52×10^{-2}
						$E2$[g]	720	$2.4(15) \times 10^{4}$	3.19×10^{4}
71.82	7/2 3/2$^+$		29.36[g]		7/2 5/2$^+$	$M1$			0.7×10^{-2}
						$E2$			3.7×10^{3}
			42.68(4)	0.5	5/2 3/2$^+$	$M1$			1.4×10^{-2}
						$E2$			1.1×10^{4}
			71.8159(20)[d]	0.40(2)	3/2 3/2$^+$	$E2$			0.7×10^{4}
			(71.82)		5/2 5/2$^+$	$M1$			0.5×10^{-2}
						$E2$			3.1×10^{3}
97.14	9/2 5/2$^+$	147(12)[e]	25.14(10)[h]	0.65(3)	7/2 3/2$^+$	$M1$	210	$3.8(4) \times 10^{-2}$	8.56×10^{-3}
			54.699(1)[g]	1.94(32)[g]	7/2 5/2$^+$	$M1$[g]	21.5	$9.2(19) \times 10^{-3}$	1.61×10^{-2}
						$E2$[g]	200	$9.3(27) \times 10^{3}$	5.13×10^{3}
			67.943(6)[g]	0.17(4)[g]	5/2 3/2$^+$	$E2$	70	$1.6(4) \times 10^{3}$	930
			97.134(1)[g]	2.17(49)[g]	5/2 5/2$^+$	$E2$	14.0	$3.4(8) \times 10^{3}$	2.09×10^{3}
125.51	9/2 3/2$^+$		(28.37)		9/2 5/2$^+$	$M1$			0.6×10^{-2}
						$E2$			3.9×10^{3}
			53.69(9)	0.12(1)	7/2 3/2$^+$	$M1$			1.3×10^{-2}
						$E2$			0.9×10^{4}
			82.957(30)[g]	0.005(1)[g]	7/2 5/2$^+$	$M1$			0.4×10^{-2}
						$E2$			3.5×10^{3}
			96.224(2)[g]	0.04(1)[g]	5/2 3/2$^+$	$E2$			0.4×10^{4}
			125.41(6)[g]	0.0018(4)[g]	5/2 5/2$^+$	$E2$			3.2×10^{3}
146.35	5/2 5/2$^-$	329(8)	74.5390(40)[d]	7.2(2)	7/2 3/2$^+$	$E1$	0.260	$3.3(1) \times 10^{-4}$	8.67×10^{-5}
			117.1628(9)[d]	15.7(5)	5/2 3/2$^+$	$E1$	0.332	$1.83(7) \times 10^{-4}$	1.00×10^{-4}
			146.3462(6)[d]	34(1)	5/2 5/2$^+$	$E1$	0.195	$2.04(8) \times 10^{-4}$	2.50×10^{-4}
148.16	7/2 5/2$^-$	689(34)	(1.81)*	$3.84(34) \times 10^{-4}$[i]	5/25/2$^-$	$M1$	8500	$2.9(3) \times 10^{-1}$	1.07×10^{-1}
			76.3507(27)[d]	0.68(2)	7/2 3/2$^+$	$E1$	0.255	$7.5(4) \times 10^{-5}$	1.34×10^{-5}
			118.9721(15)[d]	6.1(2)	5/2 3/2$^+$	$E1$	0.321	$1.8(1) \times 10^{-4}$	8.89×10^{-5}
			148.14(7)	0.62(2)	5/2 5/2$^+$	$E1$	0.192	$9.3(6) \times 10^{-6}$	7.49×10^{-6}
164.52	3/2 3/2$^-$	61(7)	(16.36)*	0.0012(2)[i]	7/2 5/2$^-$	$E2$	20000	$4.8(10) \times 10^{4}$	2.40×10^{4}
			18.17(5)[h]	0.084(14)[i]	5/2 5/2$^-$	$M1$	155	$4.6(9) \times 10^{-2}$	3.23×10^{-2}
			135.3393(5)[d]	37(1)	5/2 3/2$^+$	$E1$	0.23	$5.4(6) \times 10^{-4}$	1.24×10^{-4}
			164.5240(5)[d]	100	3/2 3/2$^+$	$E1$	0.15	$8.1(10) \times 10^{-4}$	7.86×10^{-4}
217.15	5/2 3/2$^-$	30(7)	52.71(5)	0.14(1)	3/2 3/2$^-$	$M1$	23.5	$1.0(2) \times 10^{-1}$	1.22×10^{-1}
			145.46(4)	2.1(1)	7/2 3/2$^+$	$E1$	0.195	$7.9(19) \times 10^{-4}$	8.7×10^{-4}
			187.9669(3)[d]	2.32(7)	5/2 3/2$^+$	$E1$	0.110	$4.1(10) \times 10^{-4}$	5.7×10^{-4}
			217.1519(20)[d]	3.7(1)	3/2 3/2$^+$	$E1$	0.078	$4.2(10) \times 10^{-4}$	2.9×10^{-4}
237.35	7/2 3/2$^-$	$\leqslant$34	(89.2)*	0.050(16)[i]	7/2 5/2$^-$	$M1$	5.1	$\geqslant 2.6 \times 10^{-2}$	1.51×10^{-2}
			(91.0)*	0.13(2)[i]	5/2 5/2$^-$	$M1$	4.9	$\geqslant 6.3 \times 10^{-2}$	5.90×10^{-2}
			111.4(1)	0.37(3)	9/2 3/2$^+$	$E1$	0.370	$\geqslant 1.1 \times 10^{-3}$	1.80×10^{-3}
			165.0(1)*	0.27(7)[i]	7/2 3/2$^+$	$E1$	0.145	$\geqslant 2.4 \times 10^{-4}$	2.90×10^{-4}
			208.1795(7)[d]	0.61(2)	5/2 3/2$^+$	$E1$	0.087	$\geqslant 2.7 \times 10^{-4}$	3.70×10^{-4}
			237.4(2)[h]	0.6	5/2 5/2$^+$	$E1$	0.063	$\geqslant 1.8 \times 10^{-4}$	1.10×10^{-4}
261.96	1/2 1/2$^+$	15(3)	261.958(4)[d]	38(1)	3/2 3/2$^+$	$M1$	1.18	$4.5(10) \times 10^{-2}$	2.33×10^{-2}
						$E2$	0.24	$8.2(18) \times 10^{3}$	9.21×10^{3}
288.48	3/2 1/2$^+$	16(7)	259.30(7)	9.4(4)	5/2 3/2$^+$	$M1$	1.22	$4.7(21) \times 10^{-2}$	3.80×10^{-2}
			288.5(1)	4	3/2 3/2$^+$	$M1$	0.90	$1.4(7) \times 10^{-2}$	1.21×10^{-2}

TABLE I. *(Continued.)*

Initial level (keV)	$I_i K_i^\pi$	$T_{1/2}$ (ps)	E_γ (keV)	I_γ[a]	$I_f K_f^\pi$	$X\lambda$[a]	α_{TOT}[b]	$B_{exp}(X\lambda)$[c]	$B_{theor}(X\lambda)$
303.01	7/2 7/2$^+$	110(17)	154.85(4)	0.37(2)	7/2 5/2$^-$	$E1$	0.17	$4.5(7)\times10^{-4}$	8.60×10^{-4}
			303.55(7)[h]	0.25(1)	5/2 5/2$^+$	$M1$	0.78	$3.6(6)\times10^{-3}$	2.11×10^{-3}
317.17	5/2 1/2$^+$	9.0(16)	(28.7)*	0.012(2)[i]	3/2 1/2$^+$	$M1$	140	$3.3(8)\times10^{-2}$	4.2×10^{-2}
			(55.2)*	0.006(1)[i]	1/2 1/2$^+$	$E2$	195	$1.1(3)\times10^{4}$	1.5×10^{4}
			99.95(8)	0.22(7)	5/2 3/2$^-$	$E1$	0.117	$1.6(6)\times10^{-4}$	0.9×10^{-4}
			168.94(5)	0.20(3)	7/2 5/2$^-$	$E1$	0.140	$3.0(7)\times10^{-5}$	1.7×10^{-5}
			170.8091(24)[d]	0.37(1)	5/2 5/2$^-$	$E1$	0.136	$5.3(10)\times10^{-5}$	1.7×10^{-5}
			245.3498(11)[d]	10.9(3)	7/2 3/2$^+$	$M1$	1.45	$3.0(6)\times10^{-2}$	2.5×10^{-2}
						$E2$	0.31	$4.2(9)\times10^{3}$	3.2×10^{3}
			274.79(5)	1.22(4)	7/2 5/2$^+$	$M1$	1.02	$1.8(4)\times10^{-3}$	1.2×10^{-3}
						$E2$	0.27	$3.9(2)\times10^{2}$	2.5×10^{2}
			288.04(4)	4	5/2 3/2$^+$	$M1$	0.88	$1.1(3)\times10^{-2}$	0.7×10^{-2}
			317.1689(15)[d]	23.4(7)	3/2 3/2$^+$	$M1$	0.700	$1.9(4)\times10^{-2}$	1.8×10^{-2}
						$E2$	0.140	$4.1(8)\times10^{3}$	1.2×10^{3}
320.55	5/2 5/2$^+$	10.3(21)	(32.1)*	0.012(2)[i]	3/2 1/2$^+$	$M1$	105	$3.3(9)\times10^{-2}$	2.5×10^{-2}
			(58.6)*	0.005(1)[i]	1/2 1/2$^+$	$E2$	145	$9.5(27)\times10^{3}$	5.7×10^{3}
			156.04(9)*	0.31(7)[i]	3/2 3/2$^-$	$E1$	0.167	$8.3(25)\times10^{-5}$	7.5×10^{-5}
			171.9(2)	0.26(5)	7/2 5/2$^-$	$E1$	0.135	$5.2(15)\times10^{-5}$	6.1×10^{-5}
			174.1919(20)[d]	0.43(1)	5/2 5/2$^-$	$E1$	0.130	$8.3(17)\times10^{-5}$	9.5×10^{-5}
			248.74(6)	3.9(10)	7/2 3/2$^+$	$M1$	1.40	$2.3(8)\times10^{-2}$	1.8×10^{-2}
			278.08(4)	2.55(8)	7/2 5/2$^+$	$M1$	0.98	$4.7(11)\times10^{-3}$	3.7×10^{-3}
						$E2$	0.205	$1.1(3)\times10^{3}$	0.9×10^{3}
			291.3561(9)[d]	11.0(3)	5/2 3/2$^+$	$M1$	0.85	$2.5(5)\times10^{-2}$	2.3×10^{-2}
						$E2$	0.175	$2.7(6)\times10^{3}$	1.9×10^{3}
			320.5471(13)[d]	5.9(2)	5/2 5/2$^+$	$M1$	0.68	$5.7(14)\times10^{-3}$	4.9×10^{-3}
						$E2$	0.135	$1.5(3)\times10^{3}$	1.1×10^{3}
365.81	7/2 5/2$^+$	9(4)	(45.3)*	0.037(7)[i]	5/2 5/2$^+$	$M1$	38	$8.4(41)\times10^{-2}$	9.7×10^{-2}
			(48.6)*	0.044(9)[i]	5/2 1/2$^+$	$M1$	31	$8.1(40)\times10^{-2}$	5.6×10^{-2}
			217.6(1)	0.19(5)	7/2 5/2$^-$	$E1$	0.078	$4.3(22)\times10^{-5}$	5.6×10^{-5}
			219.55(4)	0.53(2)	5/2 5/2$^-$	$E1$	0.076	$1.2(5)\times10^{-4}$	1.8×10^{-4}
			240.5(1)	1.17(3)	9/2 3/2$^+$	$M1$	1.50	$1.1(5)\times10^{-2}$	0.9×10^{-2}
						$E2$	0.32	$1.7(8)\times10^{3}$	0.7×10^{3}
			268.6747(21)[d]	1.04(3)	9/2 5/2$^+$	$M1$	1.10	$7.2(33)\times10^{-3}$	6.7×10^{-3}
						$E2$	0.23	$8.2(38)\times10^{2}$	6.5×10^{2}
			293.995(9)[d]	0.53(2)	7/2 3/2$^+$	$M1$	0.84	$4.4(20)\times10^{-3}$	3.9×10^{-3}
			323.3806(14)[d]	3.3(1)	7/2 5/2$^+$	$M1$	0.66	$5.4(25)\times10^{-3}$	7.01×10^{-3}
						$E2$	0.128	$2.1(9)\times10^{3}$	1.2×10^{3}
			336.6195(16)[d]	2.35(7)	5/2 3/2$^+$	$M1$	0.60	$3.7(19)\times10^{-3}$	2.9×10^{-3}
						$E2$	0.118	$1.2(5)\times10^{3}$	0.9×10^{3}
			365.75(4)	3.2(1)	5/2 5/2$^+$	$M1$	0.48	$1.4(6)\times10^{-2}$	1.1×10^{-2}
423.95	1/2 1/2$^-$	190(8)	135.55(7)*	1.1(2)[i]	3/2 1/2$^+$	$E1$	0.23	$1.8(3)\times10^{-4}$	1.6×10^{-4}
			162.01(5)	0.64(2)	1/2 1/2$^+$	$E1$	0.155	$6.1(3)\times10^{-5}$	5.5×10^{-5}
			259.40(3)	1.6(3)	3/2 3/2$^-$	$M1$	1.22	$3.4(6)\times10^{-3}$	2.9×10^{-3}
425.30	3/2 1/2$^-$	290(48)	163.35(5)	0.4	1/2 1/2$^+$	$E1$	0.15	$6.6(20)\times10^{-5}$	5.9×10^{-5}
			277.21(6)	0.31(4)[i]	7/2 5/2$^-$	$E2$	0.21	$1.8(4)\times10^{2}$	1.1×10^{2}
			278.7(1)*	0.49(7)[i]	5/2 5/2$^-$	$M1$	0.98	$1.5(3)\times10^{-3}$	0.9×10^{-3}
			425.36(5)[h]	0.27(1)	3/2 3/2$^+$	$E1$	0.018	$2.5(4)\times10^{-6}$	2.1×10^{-6}
478.58	5/2 1/2$^-$	$\leqslant$16	157.88(9)	0.8(2)	5/2 5/2$^+$	$E1$	0.165	$\geqslant1.5\times10^{-4}$	1.1×10^{-4}
			189.6(1)	0.09(1)	3/2 1/2$^+$	$E1$	0.11	$\geqslant9.8\times10^{-6}$	2.5×10^{-6}
			241.18(9)*	0.55(9)[i]	7/2 3/2$^-$	$M1$	1.48	$\geqslant2.6\times10^{-3}$	1.2×10^{-3}
			261.80(9)*	0.58(8)[i]	5/2 3/2$^-$	$M1$	1.18	$\geqslant2.2\times10^{-3}$	1.9×10^{-3}
			314.12(5)*	0.78(10)[i]	3/2 3/2$^-$	$M1$	0.72	$\geqslant1.7\times10^{-3}$	1.2×10^{-3}
			330.54(4)	0.49(2)	7/2 5/2$^-$	$M1$	0.63	$\geqslant9.1\times10^{-4}$	7.6×10^{-4}

TABLE I. *(Continued.)*

Initial level (keV)	$I_i K_i^\pi$	$T_{1/2}$ (ps)	E_γ (keV)	I_γ[a]	$I_f K_f^\pi$	$X\lambda$[a]	α_{TOT}[b]	$B_{exp}(X\lambda)$[c]	$B_{theor}(X\lambda)$
			332.52(4)[h]	0.09(1)	$5/2\ 5/2^-$	$M1$	0.63	$\geqslant 1.6\times10^{-4}$	0.9×10^{-4}
			406.53(8)*	3.5(6)[i]	$7/2\ 3/2^+$	$E1$	0.0195	$\geqslant 3.9\times10^{-5}$	1.7×10^{-5}
			436.20(4)[h]	5.6(2)	$7/2\ 5/2^+$	$E1$	0.017	$\geqslant 5.0\times10^{-5}$	3.8×10^{-5}
			449.17(9)	3.7(6)[i]	$5/2\ 3/2^+$	$E1$	0.0155	$\geqslant 3.0\times10^{-5}$	1.7×10^{-5}
			478.64(4)[h]	17.5(5)	$5/2\ 5/2^+$	$E1$	0.014	$\geqslant 1.2\times10^{-4}$	0.8×10^{-4}

[a] γ-ray intensities and $\delta^2(E2/M1)$ mixing ratios are from Ref. [15] except when noted otherwise.
[b] Total internal conversion coefficients for transitions with energies above 21 keV are from Ref. [21]; those for transitions with lower energies are from Ref. [22].
[c] In the units e^2 fm^2 for $E1$ transitions, e^2 fm^4 for $E2$ transitions, and μ_N^2 for $M1$ transitions.
[d] γ-ray energy adopted from Ref. [2].
[e] Lifetimes of the 42.3- and 97.1-keV levels are from Ref. [17].
[f] Individual intensities of the 42-keV doublet are deduced from $\gamma\gamma$ coincidence results and the total intensity from Ref. [15].
[g] $\delta^2(E2/M1)$ for the 42.34-keV γ ray and data concerning γ transitions de-exciting the 97.14- and 125.51-keV levels are from Ref. [23]. Intensities of γ transitions were renormalized to the units used in Ref. [15].
[h] From Ref. [15].
[i] γ-ray intensity determined in this work.

1. Slope fitting

Lifetimes longer than about 40 ps, which manifest themselves by strong asymmetry (or slope) on the delayed side of the time spectra, have been measured using the deconvolution method [18]. This method is frequently called *slope fitting* from its simplest form of analysis. Examples of such time-delayed spectra are those obtained for the 146.4-, 148.2-, and 424.0-keV levels in ^{229}Th as shown in Fig. 5. The fitted function includes four free parameters, namely position and full width at half-maximum of the Gaussian, which approximates prompt time response of the timing detectors, the half-life value, and one parameter that provides an overall renormalization between the experimental and fitted time spectra. More details on the fitting procedures are given in Ref. [18].

As an example of the analysis consider the half-life of the 146.4-keV level. As seen in Fig. 1 the 146.4-keV level is strongly fed from above by the 422.9-keV transition, which can be very clearly identified also in the corresponding BaF_2 coincident spectrum despite the poor energy resolution of the BaF_2 detectors. By reversing the gates and selecting the 422.9-keV transition in the Ge detector (see Fig. 3), one can unambiguously select in the BaF_2 spectrum the 117.2- and 146.3-keV transitions de-exciting the 146.4-keV level. Then by selecting the energy gate in this spectrum covering the full energy peaks of the 117.2- and 146.3-keV transitions, one obtains the time-delayed β-BaF_2(t) spectrum shown in the top panel of Fig. 5. We note here that all spectra shown in Figs. 1–3 and 5 were also gated on the β detector using one common energy gate. In the γ cascades selected for analysis, care was taken to ensure that γ rays feeding the state of interest from above de-excite levels with lifetimes much shorter than the measured lifetime and do not interfere in the deconvolution process.

TABLE II. New γ lines in ^{229}Th not listed in Table I.

E_γ (keV)	I_γ	Initial level (keV)
24.8(1)		661.6
69.1(2)		638.6
83.9(2)		689.0
84.8(1)		654.0
156.3(1)	1.6(6)	605.3
161.46(8)	0.53(10)	449.7
203.47(6)	0.94(12)	569.3
343.3(1)	0.18(4)	605.3
526.4(4)	2.1(8)	569.3

The time spectrum shown in Fig. 5 represents in fact a sum of similar time distributions gated in Ge detector on the 219.6-, 422.9-, and 515.2-keV transitions feeding directly the 146.4-keV level from above. The half-lives determined individually from their time distributions are the same within the uncertainties; nevertheless the contributions related to the 219.6- and 515.2-keV transitions have much weaker statistics than that for the 422.9-keV line, and thus they influence in a minor way the final value for the half-life of the 146.4-keV level.

The half-lives for the levels at 146.4, 148.2, 164.5, 303.0, 424.0, and 425.3 keV have been determined by the de-convolution method as 329(8), 689(34), 61(7), 110(17), 190(8), and 290(48) ps, respectively. These results were obtained in the second run, characterized by higher statistics and slightly better energy resolution in the Ge detectors. For a comparison we list the half-lives of $T_{1/2} = 332(18)$, 677(62), 62(11), and 175(18) ps obtained for the 146.4-, 148.2-, 164.5-, and 424.0-keV levels, respectively, in the first run. Moreover, our half-life results measured for the 146.4- and 164.5-keV levels from triple coincidence β-BaF_2-Ge events nicely confirm the values of 336(10) and 53(4) ps obtained for these levels by Gulda *et al.* [15] in a less restrictive way from double β-BaF_2(t) coincidences.

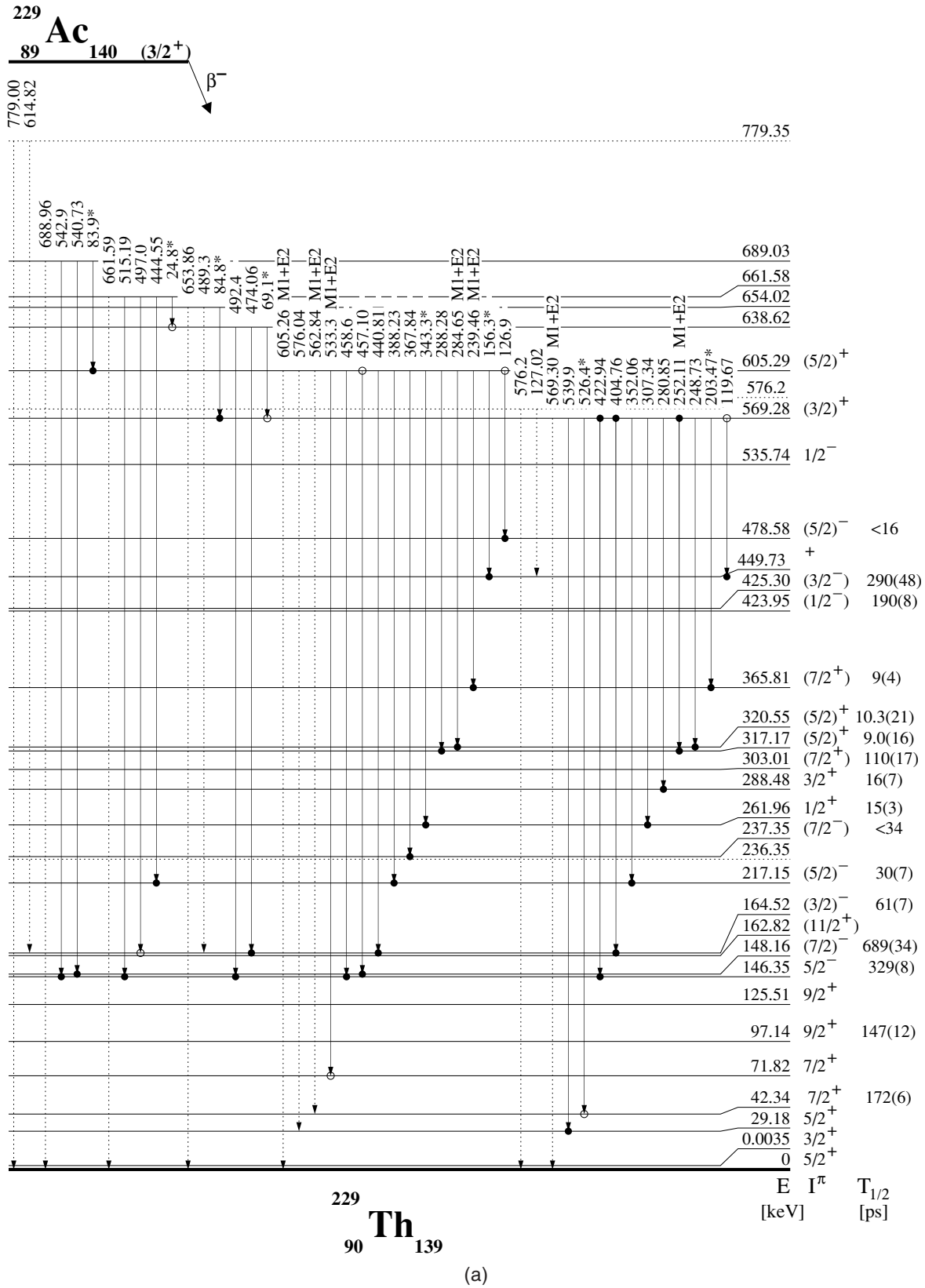

(a)

FIG. 4. The level scheme of ^{229}Th from the β decay of ^{229}Ac. Full and empty circles indicate strong and weak $\gamma\gamma$ coincidence relations, respectively. Dotted lines mark transitions seen in Ref. [15] but not observed in our data; while dashed lines show highly converted and unobserved transitions established on the basis of our coincidence relations. Stars indicate new transitions in the β decay of ^{229}Ac observed in this work. Lifetimes for the 42.3- and 97.1-keV levels are taken from Ref. [17].

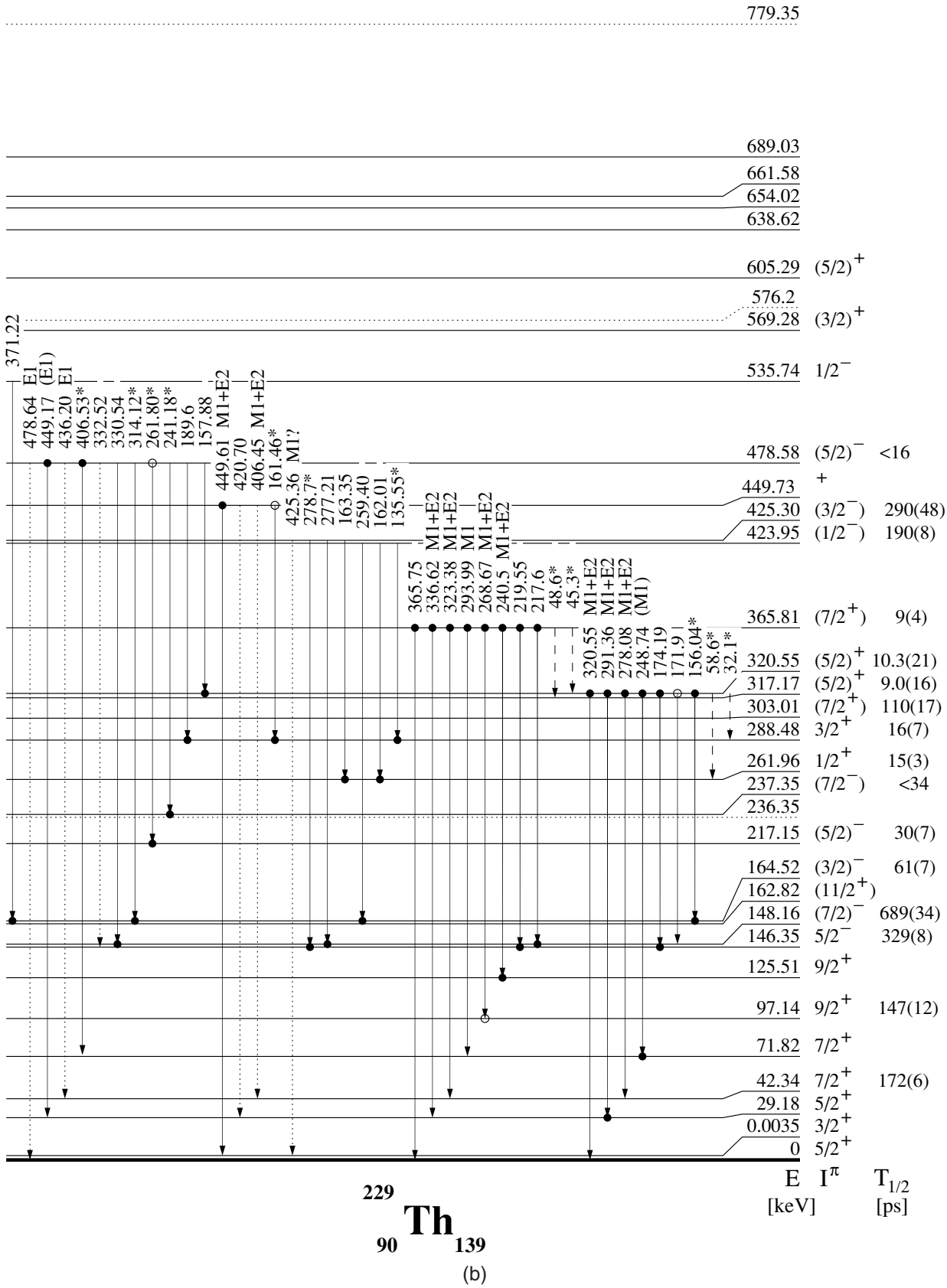

(b)

FIG. 4. *(Continued.)*

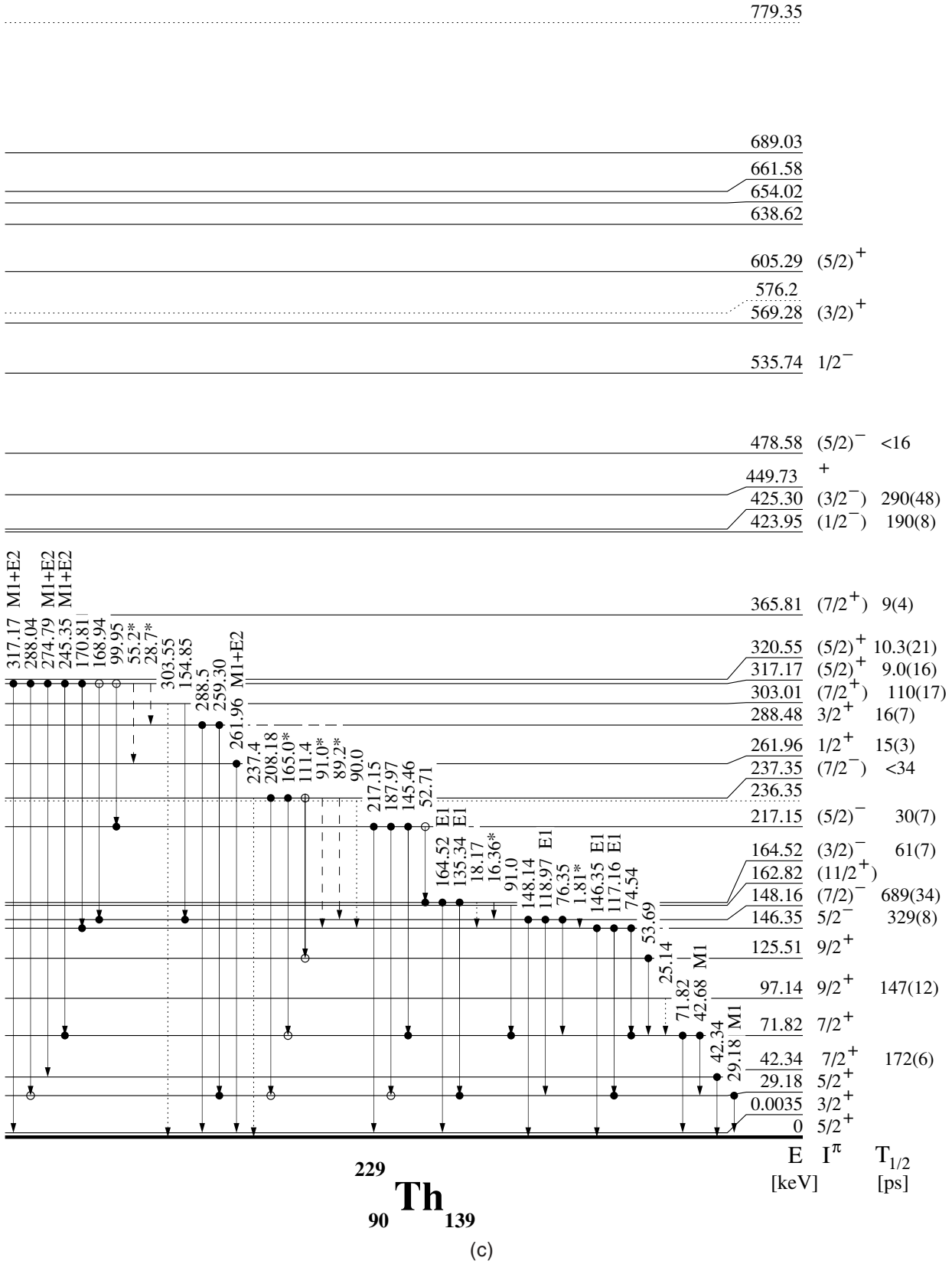

(c)

FIG. 4. *(Continued.)*

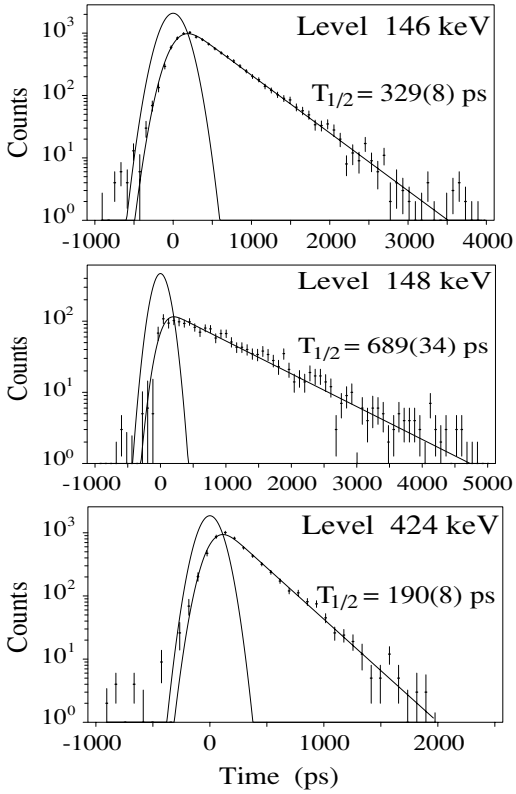

FIG. 5. Time-delayed $\beta\gamma\gamma$(t) spectra showing slopes corresponding to the lifetimes of the 146.4-, 148.2-, and 424.0-keV levels in ^{229}Th. Each figure shows experimental points, a prompt Gaussian spectrum, and a slope curve, which was fitted in the deconvolution process.

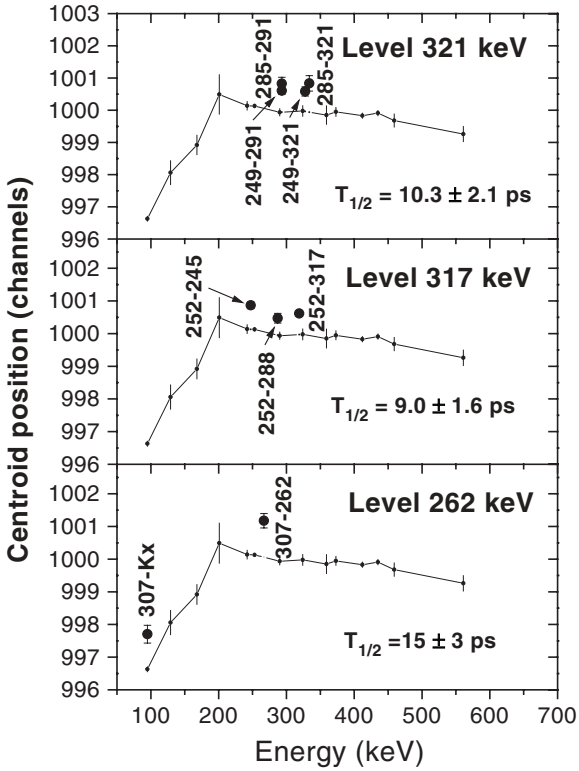

FIG. 6. Determination of half-lives for the 262.0-, 317.2-, and 320.6-keV levels by the centroid-shift technique. Each figure shows the reference curve (solid line) and centroid positions of time-delayed spectra marked by the energies (in keV) of γ-ray gates in the Ge and BaF_2 detectors. The shift of the time-delayed centroid from the reference curve gives the mean life of the level [calibration 20.00(6) ps/ch]; see text for details.

2. Centroid-shift analysis

Lifetimes shorter than 40 ps were measured using the centroid-shift method [18], in which the mean lifetime $\tau = T_{1/2}/\ln 2$ is determined as a shift of the centroid of the time-delayed spectrum from the prompt curve at a given γ-ray energy. Centroid-shift measurements in this work are based on the concept of a two γ-ray cascade [18]. The method is illustrated using an example of the 317.2-keV level, for which the shortest and the most precise result has been obtained.

Consider the cascade involving the 252.1- and 317.2-keV transitions de-exciting the 569.3-keV level to the ground state via the 317.2-keV intermediate state, the lifetime of which is to be determined. As seen in Fig. 2, by gating on the 317.2-keV transition in the Ge detector, one is able to select the very strong 252.1-keV transition in the BaF_2 spectrum and determine the centroid position of the resultant time-delayed β-$BaF_2(t)$ spectrum. This position represents our reference point, which is shown on the *reference curve* in Fig. 6 at the energy of 252 keV. [Similarly, one can use the time spectrum generated by the 245.3-keV (Ge) and the 252.1-keV (BaF_2) gates (see Fig. 1), to confirm the reference point at 252 keV.] We do not know the lifetime of the 569.3-keV level or levels above it, which feed this state. For the purpose of the present analysis these lifetimes do not have to be determined since they cancel out in the analysis.

By reversing the gates and selecting the 252.1-keV transition in the Ge detector (see Fig. 2), one can gate on the full energy peaks of the 245.3- and 317.2-keV γ rays de-exciting the 317.2-keV level. By selecting these transitions in the BaF_2 energy spectrum one obtains the time-delayed β-$BaF_2(t)$ distributions, the centroids of which are shifted from the reference point by exactly the mean life of the 317.2-keV level. As shown in the middle panel of Fig. 6 these points, labeled 252–245 and 252–317, are shifted above the reference curve.

As seen in the figure, a single reference point at one γ-ray energy (say at 252 keV) will not allow for a precise lifetime determination if the time-shifted point is measured at another energy (say 317 keV), unless a reference curve is established over a wider energy range. A second point can be easily established at 423 keV by using the Ge gate at 146.3 keV and selecting the 422.9-keV transition in the BaF_2 spectrum (see Fig. 1). Since this transition de-excites the same 569.3-keV level as the 252.1-keV γ ray, the centroid of the time spectrum selected with the 146.3-keV (Ge) and 422.9-keV (BaF_2) transitions represents exactly the position of the reference curve at 423 keV. We note that the reference curve is relatively flat in the energy range from 252 to 423 keV, which would allow us to complete the measurement for the 317.2-keV level using only two reference points. However, by using different combinations of gates set on the full-energy peaks in the Ge and BaF_2 spectra on transitions de-exciting

the 569.3-keV level we have extended the reference curve. Moreover, a similar curve was established for transitions de-exciting the 605.3-keV level. Since, within the high level of precision, there was no detectable shift between these curves we have merged them into one reference curve shown in Fig. 6.

We have used three time-delayed points to determine the half-life of the 317.2-keV state. The third point was set at an energy of 288 keV in the BaF_2 spectrum. This gate includes not only the full energy peak of the 288.0-keV γ ray but also contributions from other weaker lines at this energy and a partial contribution from the full energy peaks at 245.3 and 317.2 keV. Since all these transitions de-excite the same level at 317.2 keV and contribution from the Compton tail is minor at these energies, there was no need for any correction procedures.

We finally note that since all time-delayed spectra were started with the detection of a β particle, the gating conditions on the β spectrum were chosen to keep the time response of the β detector constant to within $\sim$1 ps over the range of selected β particle energies.

3. Transition rates

Half-life results obtained in the present work are shown in the level scheme and are listed in the third column of Table I. Reduced transition probabilities for about 70 transitions in ^{229}Th are given in column 9 of Table I. Most of them were established in this work. They were determined from level lifetimes and relative γ-ray intensities using total internal conversion coefficients from Ref. [21]. For transitions with energies below 21 keV total internal conversion coefficients were taken from Ref. [22]. For the 1.8-keV transition, assumed to be of $M1$ type, a total internal conversion coefficient of $\alpha_{tot} = 8500$ was estimated by extrapolation of values listed in Ref. [22].

IV. DISCUSSION

A. Single quasiparticle configurations in ^{229}Th

The occurrence of strong octupole correlations in odd-A nuclei is manifested by the presence of parity doublet bands and enhanced $E1$ transitions between members of these bands. This effect persists in the ocupole soft nuclei where significant octupole coupling may exist between selected close-lying bands of opposite parity. For this reason these bands are labeled *parity partner bands* [24] (see also the discussion in Sec. IV C).

In the case of parity doublet $K^\pi = 1/2^\pm$ bands the decoupling parameters are expected to be of equal magnitudes and opposite signs. According to the single quasi-particle calculations performed by Ćwiok and Nazarewicz [25,26] for ^{229}Th, one expects nine single-particle states below 1 MeV: three states with $K = 1/2$, two with $K = 3/2$, three with $K = 5/2$, and one with $K = 7/2$. Our single-particle calculations (see Sec. IV E) predict one more $K = 7/2$ level at a similar, although slightly higher, excitation energy.

The configuration assignment to the five rotational bands built on the $K = 3/2$ and $K = 5/2$ states (see Fig. 7) has already been made in earlier studies [8,13,15,27]. Furthermore, the 1/2[631] and 1/2[501] configurations have been assigned to the rotational bands built on two $K = 1/2$ levels at energies of 262.0 and 535.7 keV, respectively. Recently, in an α-decay study [16] the 317.2-keV level has been proposed as the $5/2^+$ member to the first $K = 1/2$ band. The decoupling parameter a for this band is found to be equal to 0.21 and can be compared to the theoretical value of 0.30 predicted by Leander and Chen

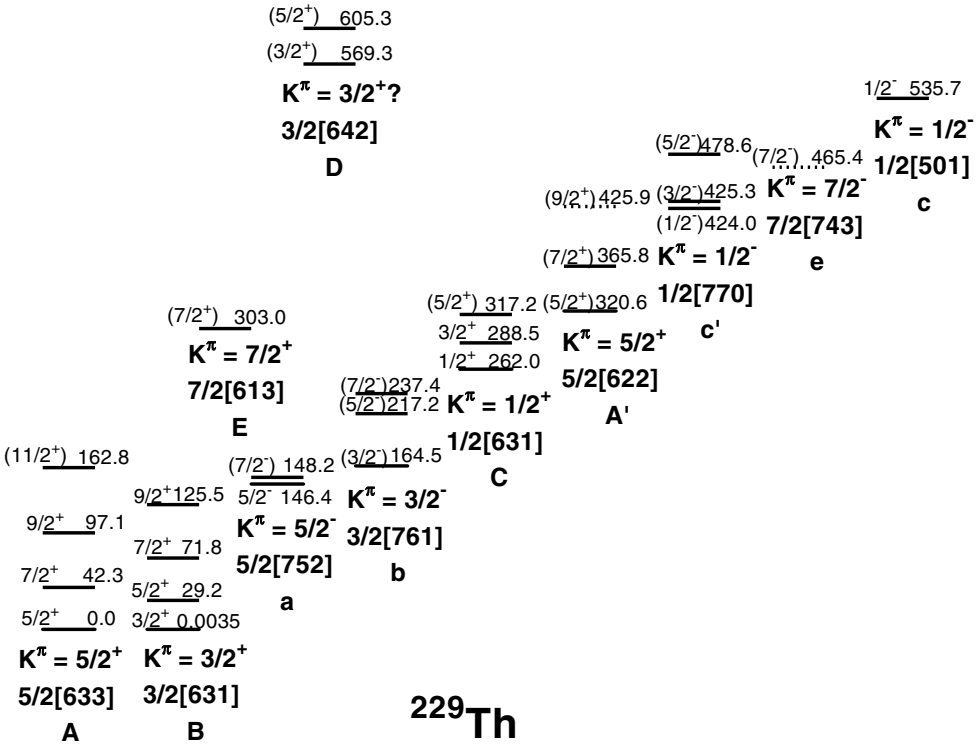

FIG. 7. Experimental levels in ^{229}Th grouped into rotational bands. Dashed lines represent levels populated in the α decay [8,9,16]. Each band is labeled by the dominant single-quasiparticle component of the wave function as obtained in the calculations in Sec. IV C. The structure of the intrinsic states forming the base for each rotational band is given in Table III. The pairs of bands labeled by the same small and capital letters are interpreted as parity partner bands.

TABLE III. Structure of the intrinsic states in ^{229}Th calculated within the quasiparticle-plus-phonon model. The band labels are the same as in Fig. 7.

Band label	Structure of the wave function
A	$5/2[633](84\%) + (5/2[752] + Q_{30}^{+})(4\%)$ $+(5/2[503] + Q_{30}^{+})(2\%)$
A'	$5/2[622](85\%) + 5/2[633](1\%) + (5/2[752] + Q_{30}^{+})(5\%)$
B	$3/2[631](43\%) + 3/2[642](31\%) + (3/2[761] + Q_{30}^{+})(12\%)$
C	$1/2[631](57\%) + 1/2[640](11\%) + 1/2[651](7\%)$ $+(1/2[770] + Q_{30}^{+})(8\%) + (1/2[501] + Q_{30}^{+})(2\%)$
D	$3/2[642](43\%) + 3/2[631](28\%) + (3/2[761] + Q_{30}^{+})(19\%)$ $+(3/2[501] + Q_{30}^{+})(3\%)$
E	$7/2[613](39\%) + 7/2[624](37\%) + (7/2[743] + Q_{30}^{+})(12\%)$
a	$5/2[752](83\%) + 5/2[503](1\%) + (5/2[633] + Q_{30}^{+})(11\%)$
b	$3/2[761](80\%) + (3/2[642] + Q_{30}^{+})(14\%)$ $+(3/2[651] + Q_{30}^{+})(2\%)$
c	$1/2[501](77\%) + 1/2[770](1\%) + (1/2[651] + Q_{30}^{+})(9\%)$ $+(1/2[640] + Q_{30}^{+})(5\%) + (1/2[660] + Q_{30}^{+})(3\%)$
c'	$1/2[770](70\%) + 1/2[501](8.2\%) + (1/2[640] + Q_{30}^{+})(9.3\%)$
e	$7/2[743](75\%) + (7/2[624] + Q_{30}^{+})(18\%)$

[28] and to 0.285 obtained in the calculations of Sec. IV C. The $B(E2)$ value of $1.1(3) \times 10^4$ $e^2\,\mathrm{fm}^4$ deduced from our data for the 55.2-keV intraband transition gives for this band the quadrupole moment of 7.4(9) e b and the quadrupole deformation parameter $\beta_2 = 0.20$. The latter value is close to the β_2 equilibrium deformation of 0.18 obtained in our calculations of Sec. IV E for the configuration with 1/2[631] as the main component. The magnetic $|g_K - g_R|(1 - b)$ factor determined for this $K = 1/2$ band from the $B(M1)$ value of the 28.7-keV transition is equal to 1.18(14) (see Table IV). Here b denotes the magnetic decoupling parameter as defined by Eqs. (4–85) and (4–86) in Ref. [29].

The only new information obtained in this work for the second $K = 1/2$ band built on the 535.7-keV level is the theoretical value of the decoupling parameter $a = 0.27$, predicted in our calculations of Sec. IV C.

TABLE IV. Magnetic g factors for the rotational bands in ^{229}Th.

Band K^π	E_i (keV)	E_γ (keV)	I_i	$\lvert g_K - g_R\rvert$
$5/2^+$	42.34	42.34	$7/2^+$	0.24(3)[a]
	97.14	54.699	$9/2^+$	0.14(2)[a]
$5/2^-$	148.16	1.81	$7/2^-$	0.95(5)
$3/2^-$	217.15	52.71	$5/2^-$	0.84(10)
$1/2^+$	317.17	28.7	$5/2^+$	1.18(14)[b]
$5/2^+$	365.81	45.3	$7/2^+$	0.51(12)

[a]From data in Ref. [23].

[b]$|g_K - g_R|(1 - b)$, where b is the magnetic decoupling parameter.

Based on our new data, we propose the 424.0-keV ($1/2^-$) level as the head of the third $K = 1/2$ band with the 425.3-keV state as the $3/2^-$ band member. The proposed interpretation conflicts with the $M1$ multipolarity given [15] to the 425.4-keV transition. We note, however, that the 425.4-keV transition was assigned to this level based on an energy match and not on $\gamma\gamma$ coincidences; thus its assignment to this state is not firm. Moreover, if the parity assignment to the 425.3-keV level would be positive, then the 277.2-keV transition to the $7/2^-$ state would be of $M2$ type, which is very unlikely. For the $5/2^-$ member of this band we propose the 478.6-keV level. The decoupling parameter a obtained for this band is equal to -0.92 and may be compared to the theoretical value of -1.4 obtained from calculations of Sec. IV C. These calculations give 1/2[770] as the main component of the intrinsic wave function for this band. In view of the potential energy calculations from Sec. IV E the intrinsic state with this wave function component is predicted to be octupole deformed and this band could be a candidate for the negative-parity member of the $K = 1/2$ parity doublet bands.

For the 478.6-keV level we prefer the $5/2^-$ assignment proposed here, instead of the $7/2^-$ one given in Ref. [15] since then the 189.6-keV transition would become an unreasonably fast $M2$ line. Moreover, we do not observe either the 315.39- or the 381.54-keV transition to de-excite this state, as proposed in [16].

The 303.0-keV level has been tentatively interpreted in Ref. [16] as the head of the $K^\pi = 7/2^+$ band. This band may originate from the 7/2[613] configuration. A second $K = 7/2$ configuration, which originates from the 7/2[743] orbital, is predicted to be octupole deformed (see Sec. IV E). We tentatively propose the 465.4-keV level as one of the parity doublet band-heads assigned to this configuration. This level is populated in the α decay of ^{233}U [16] and de-excites to the $7/2^+$ state at 303.0 keV via a 162.5-keV transition.

Table V shows a comparison of the experimental branching ratios for $E1$ transitions to and $M1$ transitions to the theoretical intensity ratios given by Alaga's rule [30]. A good agreement is observed only for the $E1$ transitions connecting levels from the $K^\pi = 3/2^-$ band at 164.5 keV with levels of the $K^\pi = 3/2^+$ band at 0.0035 keV (see lower part of Table V). This confirms the K^π assignment for these bands. For other bands a clear deviation from the Alaga rule is observed, suggesting that most of the bands in ^{229}Th are strongly Coriolis mixed.

Theoretical branching ratios for the Coriolis coupled bands are described by the Mikhailov rule [31]. In practice, this rule can be applied to experimental data only when $|K_f - K_i| \geqslant \lambda$ and when the degree of K-forbiddenness $n = 0$. Only in this case does the Mikhailov rule take a simple form

$$B(X\lambda) = M_{if}^2 \langle I_i K_i \lambda (K_f - K_i) | I_f K_f \rangle^2 \times [1 + [I_f(I_f + 1) - I_i(I_i + 1)]]^2 a_M^2,$$

with one free parameter, a_M. As can be seen in the upper part of Table V this rule nicely reproduces branching ratios for the $E1$ transitions between $K^\pi = 5/2^-$ and $K^\pi = 3/2^+$ bands with bandheads at 146.4 and 0.0035 keV, respectively. For this comparison, the value of a_M was set to 0.323.

TABLE V. Comparison of experimentally obtained branching ratios for the $E1$ transitions in ^{229}Th to the Alaga and Mikhailov rules.

Initial level (keV)	I_i^π K_i	I_f^π K_f	E_γ (keV)	Reduced branching ratios		
				Exp	Theory	
					Alaga	Mikhailov[a]
146.35	$5/2^-$ 5/2	$5/2^+$ 3/2	117.16	1	1	1
		$7/2^+$ 3/2	74.54	1.78(8)	0.17	1.78
148.16	$7/2^-$ 5/2	$5/2^+$ 3/2	118.97	1	1	1
		$7/2^+$ 3/2	76.35	0.42(2)	0.71	0.45
164.52	$3/2^-$ 3/2	$3/2^+$ 3/2	164.52	1	1	
		$5/2^+$ 3/2	135.34	0.66(3)	0.67	
217.15	$5/2^-$ 3/2	$3/2^+$ 3/2	217.15	1	1	
		$5/2^+$ 3/2	187.97	0.97(4)	0.96	
		$7/2^+$ 3/2	145.46	1.89(10)	1.79	
237.35	$7/2^-$ 3/2	$5/2^+$ 3/2	208.18	1	1	
		$7/2^+$ 3/2	165.0	0.9(2)	0.40	
		$9/2^+$ 3/2	111.4	4.0(4)	1.40	

[a]Obtained using parameter $a_M = 0.323$.

B. $B(E1)$ rates

A common property of nuclei with strong octupole correlations is the presence of enhanced $E1$ transitions. A significant number of reduced transition probabilities $B(E1)$ listed in column 9 of Table I are moderately fast, of the order of $10^{-4}\,e^2\,\mathrm{fm}^2$, whereas typical $B(E1)$ values for nuclei from nonoctupole collective regions are much slower, below $10^{-5}\,e^2\,\mathrm{fm}^2$. In particular, the $E1$ transitions connecting members of the $K^\pi = 3/2^\pm$ bands with bandheads at 0.0035 and 164.5 keV have $B(E1)$ values higher than $1.8 \times 10^{-4}\,e^2\,\mathrm{fm}^2$. Evidently, these bands constitute a pair of parity partner bands. The $E1$ transitions between parity partner bands with $K^\pi = 5/2^\pm$ and $1/2^\pm$ are significantly less enhanced. No clear difference is observed between $E1$ transitions connecting the parity partner bands (intraband transitions) and those connecting opposite parity bands with different K (interband transitions). The $B(E1)$ values for many $E1$ interband transitions with $|\Delta K| = 1$ are of the order $10^{-4}\,e^2\,\mathrm{fm}^2$. This provides another indication that rotational bands in ^{229}Th are strongly mixed since mixing would enhance the interband transitions to the values comparable to those for the intraband.

A generally adopted way of comparison of the $E1$ strength over a wider range of nuclei is offered by the intrinsic electric dipole moment $|D_0|$, which removes the spin dependence affecting the $B(E1)$ rates. Assuming a strong-coupling limit and an axial shape of the nucleus, the electric dipole moment $|D_0|$ is defined (for $K \neq 1/2$) via the rotational formula

$$B(E1) = \frac{3}{4\pi} D_0^2 \langle I_i K 10 | I_f K \rangle^2.$$

It should be emphasized that the $|D_0|$ moment remains a convenient parameter for the inter-comparison even though this rotational formula may not be strictly applicable to such an octupole transitional nucleus as ^{229}Th.

Table VI provides the $|D_0|$ moments deduced from the $B(E1)$ values given in Table I for the parity partner bands in ^{229}Th. The highest $|D_0|$ values of 0.077(3) e fm (on average) are obtained for the $E1$ transitions connecting the $K^\pi = 3/2^\pm$ bands. Much smaller average $|D_0|$ values of 0.024(5) and 0.029(1) e fm are deduced for the $K^\pi = 5/2^\pm$ and $1/2^\pm$ bands, respectively. Figure 8 shows a comparison of the $|D_0|$ values from Table VI to those for the $K^\pi = 1/2^\pm$, $3/2^\pm$, and $5/2^\pm$ parity doublet or parity partner bands in other odd-A isotopes of Th. They may also be compared to the average values of

TABLE VI. Intrinsic dipole moments, $|D_0|$, for the $E1$ transitions in ^{229}Th.

E_i (keV)	$I_i^\pi K_i$	E_γ (keV)	$I_f^\pi K_f$	$\lvert D_0\rvert$ (e fm)
146.35	$5/2^-$ 5/2	146.35	$5/2^+$ 5/2	0.0345(7)
148.16	$7/2^-$ 5/2	148.14	$5/2^+$ 5/2	0.0135(4)
164.52	$3/2^-$ 3/2	135.34	$5/2^+$ 3/2	0.075(4)
		164.52	$3/2^+$ 3/2	0.075(5)
217.15	$5/2^-$ 3/2	145.46	$7/2^+$ 3/2	0.084(10)
		187.97	$5/2^+$ 3/2	0.081(10)
		217.15	$3/2^+$ 3/2	0.081(10)
237.35	$7/2^-$ 3/2	111.4	$9/2^+$ 3/2	$\geqslant$0.095
		165.0	$7/2^+$ 3/2	$\geqslant$0.084
		208.18	$5/2^+$ 3/2	$\geqslant$0.057
320.55	$5/2^+$ 5/2	171.9	$7/2^-$ 5/2	0.028(4)
		174.19	$5/2^-$ 5/2	0.022(2)
365.81	$7/2^+$ 5/2	217.6	$7/2^-$ 5/2	0.021(6)
		219.55	$5/2^-$ 5/2	0.048(11)
423.95	$1/2^-$ 1/2	135.55	$3/2^+$ 1/2	0.034(3)[a]
		162.01	$1/2^+$ 1/2	0.028(1)[a]
425.30	$3/2^-$ 1/2	163.55	$1/2^+$ 1/2	0.029(4)[a]
478.58	$5/2^-$ 1/2	189.6	$3/2^+$ 1/2	$\geqslant$0.010[a]

[a]With the D_1 term neglected (for definition of D_1 see Eq. (67) in Ref. [32]).

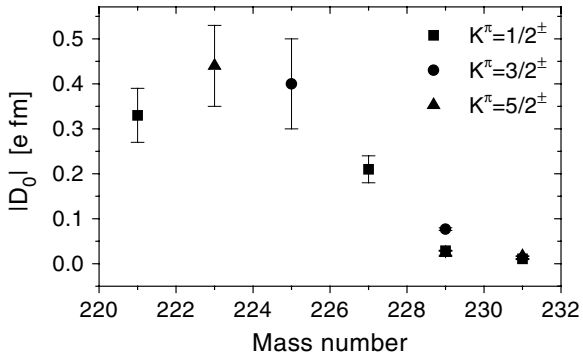

FIG. 8. Electric dipole moments for the $K^\pi = 1/2^\pm, 3/2^\pm$, and $5/2^\pm$ parity doublet or parity partner bands in the odd-A thorium isotopes. Experimental data are from Refs. [24,32,36–38] and from this work.

$|D_0| = 0.10\,e$ fm and $|D_0| \geqslant 0.11\,e$ fm for the $K^\pi = 3/2^\pm$ and $1/2^\pm$ bands in ^{227}Ra [33], the isotone of ^{229}Th, respectively, and to the $|D_0|$ values for the $K^\pi = 0^\pm$ bands in ^{228}Th and ^{230}Th, where $|D_0| = 0.121(3)\,e$ fm and $0.053(2)\,e$ fm, respectively, were determined from the $B(E1)/B(E2)$ ratios measured in [34] and the Q_0 values taken from [35]. One may conclude that the $|D_0|$ moments in ^{229}Th follow the smoothly decreasing trend of these values when moving from the center of the octupole collective region to the heavier reflection-symmetric thorium isotopes. Moreover, the difference between the intra- and interband $E1$ transitions diminishes with the decreasing strength of the octupole correlations.

C. Quasiparticle-plus-phonon model calculations

The experimental $B(E1)$ rates, as well as rates for the $E2$ and $M1$ transitions, are compared to the results of the quasiparticle-plus-phonon model (QPPM) calculations in columns 9 and 10 of Table I, respectively.

In the strong correlation limit octupole correlations lead to a stable octupole deformation of the nuclear mean field (nonzero value of the intrinsic dipole moment $|D_0|$). In the weak octupole correlation limit these correlations are not strong enough to form stable octupole deformation but are sufficiently strong to shift octupole vibrations in even-even nuclei to very low excitation energies. In the corresponding odd-A nuclei these correlations manifest themselves by relatively large octupole vibrational components in the lowest excited states. The best description of this situation is provided by the QPPM (see Refs. [24,33,39] and citations therein), where the lowest intrinsic states in odd-A nuclei are understood as the linear combinations of quasiparticle and quasiparticle-plus-phonon components. In such a way the QPPM takes into account an odd quasiparticle and vibrating even-even core. For nuclei from the region of weak octupole correlations the lowest even-even core vibrations have an octupole character.

The QPPM Hamiltonian consists of intrinsic and rotational parts (with the inclusion of Coriolis mixing). The intrinsic part of the Hamiltonian describes intrinsic states of a nucleus whereas the rotational part creates rotational bands built on top of those states. The rotational bands are mixed by the Coriolis interaction. In our calculations the intrinsic Hamiltonian involves a phenomenological mean field of the Nilsson type (with axial quadrupole and hexadecapole deformations), monopole pairing residual interactions, and long-range residual interactions in the quadrupole-quadrupole and octupole-octupole form (for details see, e.g. [24,40,41]). Appropriate choice of the model parameters gives a good agreement between the calculated energy spectrum and the experimental one as shown in Fig. 7 (see also Figs. 8 and 9 in Ref. [15]). Contributions from dominant quasiparticle and quasiparticle-plus-phonon components into each intrinsic state are listed in Table III. It can be seen that octupole phonons play a significant role in this nucleus. Moreover, one can recognize some kind of a parity doublet structure among the bands in the sense that we can indentify two bands, one of positive parity (labeled with a capital letter) and a corresponding negative-parity partner (labeled with a corresponding lowercase letter). In each such pair of bands (e.g., A-a or B-b), which we define as *parity partner bands*, the dominating single-quasiparticle component of one band forms the dominating collective quasiparticle-plus-octupole-phonon (Q^+_{30}) component of the second band, and vice versa. In such a way the QPPM reflects the parity doublet structure, which is a characteristic feature of strong octupole correlations.

One observes a very good agreement between the experimental reduced transition probabilities $B_{\rm exp}(X\lambda)$ and the theoretical values $B_{\rm theor}(X\lambda)$ calculated in the framework of the QPPM with Coriolis mixing (see Table I). The QPPM approach provides a good description of the reduced probabilities even in the case of interband transitions, because of the inclusion of octupole correlations in the residual interactions and because Coriolis mixing is taken into account. The drawback of the QPPM model in the form applied here is that it does not involve the residual interactions entirely and the vibrations of the even-even core are treated only on the RPA harmonic level (i.e., anharmonic effects are neglected).

D. Half-life of the low-energy $3/2^+$ isomer

For the $M1$ γ-ray transition connecting the low-energy $3/2^+$ level and the $5/2^+$ ground state, the QPPM calculations yield the reduced probability $B(M1) = 0.025\ \mu_N^2$ (see Table I). The half-life of this transition, expressed in hours, can be obtained from the relation $T_{1/2} = (10.95\,\text{h})/E_\gamma^3 B(M1)$, where E_γ is given in eV. The assumption of $E_\gamma = (3.5 \pm 1.0)$ eV [2] leads to $T_{1/2} = 10^{+18}_{-5}$ h, whereas by using the recently re-evaluated energy value of $E_\gamma = (5.5 \pm 1.0)$ eV [3] one obtains $T_{1/2} = 2.6^{+2.2}_{-1.0}$ h. A comparison of model predictions to an experimental half-life of the isomer, when a reliable $T_{1/2}$ value becomes available, would require a correction for the effect of an electronic bridge [42], which is an additional decay channel for the isomer.

Within our experimental approach, the half-life measurement of the isomeric state was not possible. Earlier, two groups attempted to determine this half-life using radiochemical and α-spectroscopy techniques. Browne *et al.* [6] separated the activity of ^{229}Th, and presumably of ^{229}Th^m, from a sample of ^{233}U and searched for a short-lived α-ray component originating from the decay of the isomer. The result of that experiment was negative. It has been concluded that the

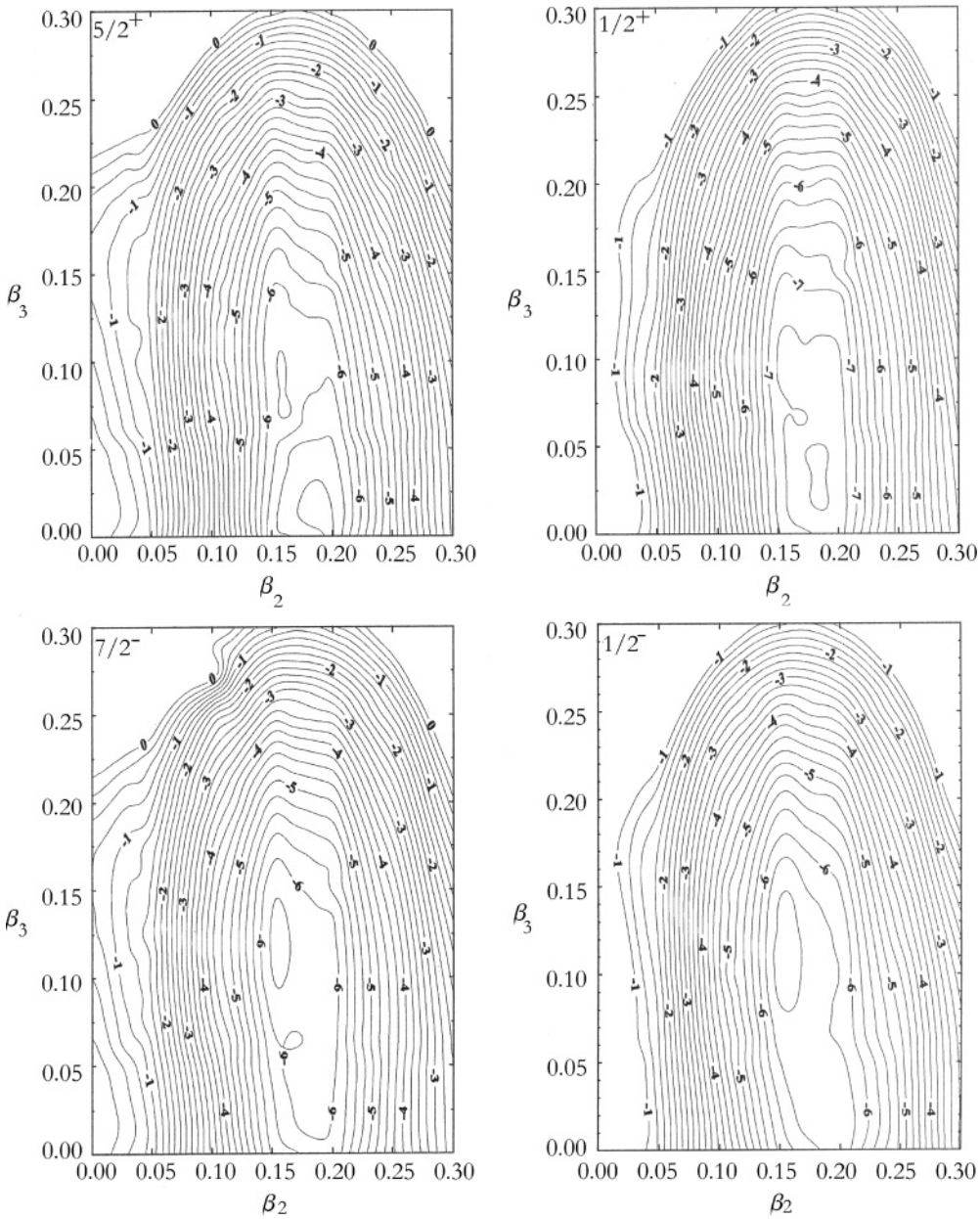

FIG. 9. Potential energy surfaces calculated for the $K^\pi = 5/2^+$ ground state (upper left panel), for two $K = 1/2$ bands with bandheads at 262.0 and 424.0 keV (upper right and lower right panels, respectively), and for the $K = 7/2$ band with bandhead at 465.4 keV (lower left panel). The energy distance between the contour lines is equal to 0.25 MeV.

^{229}Th^m half-life must be either shorter than 6 h or longer than 20 days. This conclusion conflicts with the results reported by Mitsugashira *et al*. [43]. In the latter work, the ^{229}Th^m activity was sought by producing it through the (γ,n) reaction on a ^{230}Th target. The α spectrum of the chemically separated thorium fraction was measured as a function of time. The half-life observed for the component at about 5 MeV (the energy of the α radiation expected for ^{229}Th^m) was found to be 13.9 ± 3.0 h. This value assigned to the isomer is compatible with our predictions based on the isomer energy of 3.5 ± 1.0 eV. However, in view of the disagreement between the results obtained by the two groups, further efforts to measure the half-life of the isomer are obviously needed. In Ref. [43], a study of the α decay of ^{229}Th^m after β decay of ^{229}Ac has been suggested. A stringent test of the model predictions would also require a more accurate determination of the isomer energy.

E. Potential energy surfaces

Octupole correlations can be accounted for in an alternative approach by the including octupole deformation parameter β_3 into the model calculations.

We have calculated bandhead energies and potential energy surfaces on the (β_2, β_3) plane for the lowest quasiparticle configurations in ^{229}Th. The calculations were performed using the Strutinsky method, in which the macrosopic energy contribution is obtained using the liquid-drop formula with the surface diffuseness term [44], whereas a shell correction is calculated using the axially deformed Woods-Saxon potential with the universal set of parameters [45]. Potential energy surfaces for specific configurations (see Fig. 9) have been obtained by blocking the odd neutron in state with a given K and by minimization of total energy with respect to the shape parameters $\beta_4-\beta_6$. These calculations show that for all considered configurations the quadrupole deformation β_2 is within the range of 0.15–0.20. Moreover, they show that the ^{229}Th nucleus is reflection symmetric or slightly octupole soft in all single quasiparticle configurations with spins 3/2 and 5/2. Distinct octupole softness is predicted for two $K = 1/2$ configurations with the dominating 1/2[631] and 1/2[501] single-particle components. An octupole deformation of $\beta_3 \sim 0.12$ is expected only for the $K = 7/2$ configuration with the main component 7/2[743] and for the $K = 1/2$ configuration with 1/2[770] as the main component. However, the octupole minima are not very deep and octupole barrier heights are lower than 0.5 MeV.

These calculations do not explain why enhanced $E1$ transitions are observed for the $K^\pi = 3/2^\pm$ configurations and why such transitions are weaker for the $K^\pi = 5/2^\pm$ and $K^\pi = 1/2^\pm$ bands.

Potential energy calculations performed for two odd-A neighbors of ^{229}Th show that the ^{227}Th nucleus is reflection-asymmetric in all but one lowest configuration whereas no octupole deformation is predicted for ^{231}Th. Only two configurations in the latter nucleus are foreseen to be octupole soft. Thus one concludes that ^{229}Th lies at the border of the actinide octupole collective region and coexistence of the reflection-asymmetric and reflection-symmetric shapes is predicted in this nucleus.

V. SUMMARY

The advanced time-delayed $\beta\gamma\gamma(t)$ method has been used to measure half-lives of 14 excited states in ^{229}Th. Reduced transition probabilities were obtained for more than 70 transitions. Twenty-seven new γ lines have been introduced into the decay scheme of ^{229}Ac. Enhanced $E1$ transitions are observed between the $K^\pi = 3/2^\pm$ bands.

A good agreement between experimental transition probabilities and results of the QPPM calculations implies an octupole-vibrational nature of the lowest configurations in ^{229}Th and a strong Coriolis coupling of the $K^\pi = 3/2^-$ and $K^\pi = 1/2^-$ bands. This indicates that one can describe the low-lying states in ^{229}Th without the stable octupole deformation in the mean field. The octupole softness is also confirmed by the potential energy surface calculations. A nonzero octupole deformation is foreseen only for one $K = 1/2$ and one $K = 7/2$ state lying at higher excitation energies.

Our results confirm the location of the ^{229}Th nucleus at the border of the collective octupole region in actinides where interplay takes place between reflection-symmetric and asymmetric configurations.

ACKNOWLEDGMENTS

This work has been supported in part by Grant No. 1 P03B 059 27 from the Polish Committee for Scientific Research (KBN) (for theoretical calculations), the Swedish Research Council, the research plan MSM0021620834 provided by the Ministry of Education of the Czech Republic, and the Spanish CICYT under Project No. FPA2002-04181-C04-02. Support by the European Commission through the HPRI-CT-1999-00018 project and by the ISOLDE Collaboration are also acknowledged. Fast timing detectors and electronics have been provided by the Fast Timing Pool of Electronics. One of us (E.R.) would like to thank the OSIRIS group for its generous hospitality and for financial support during her stay in Studsvik.

[1] G. A. Leander and R. K. Sheline, Nucl. Phys. **A413**, 375 (1984).
[2] R. G. Helmer and C. W. Reich, Phys. Rev. C **49**, 1845 (1994).
[3] Z. O. Guimaraes-Filho and O. Helene, Phys. Rev. C **71**, 044303 (2005).
[4] F. F. Karpeshin, S. Wycech, I. M. Band, M. B. Trzhaskovskaya, M. Pfützner, and J. Żylicz, Phys. Rev. C **57**, 3085 (1998).
[5] E. V. Tkalya, A. N. Zherikhin, and V. I. Zhudov, Phys. Rev. C **61**, 064308 (2000).
[6] E. Browne, E. B. Norman, R. D. Canaan, D. C. Glasgow, J. M. Keller, and J. P. Young, Phys. Rev. C **64**, 014311 (2001).
[7] K. Pachucki, S. Wycech, J. Żylicz, and M. Pfützner, Phys. Rev. C **64**, 064301 (2001).
[8] L. A. Kroger and C. W. Reich, Nucl. Phys. **A259**, 29 (1976).
[9] M. J. Canty, R. D. Connnor, D. A. Dohan, and B. Pople, J. Phys. G **3**, 421 (1977).
[10] K. Chayawattanangkur, G. Herrmann, and N. Trautmann, J. Inorg. Nucl. Chem. **35**, 3061 (1973).
[11] I. Ahmad, J. E. Gindler, R. R. Betts, R. R. Chasman, and A. M. Friedman, Phys. Rev. Lett. **49**, 1758 (1982).
[12] Y. A. Ellis, Nucl. Data Sheets **6**, 257 (1971).
[13] D. G. Burke, P. E. Garret, T. Qu, and R. A. Naumann, Phys. Rev. C **42**, R499 (1990).
[14] C. E. Bemis Jr., F. K. McGowan, J. L. C. Ford Jr., W. T. Milner, R. L. Robinson, P. H. Stelson, G. A. Leander, and C. W. Reich, Phys. Scr. **38**, 657 (1988).
[15] K. Gulda, W. Kurcewicz, A. J. Aas, M. J. G. Borge, D. G. Burke, B. Fogelberg, I. S. Grant, E. Hagebø, N. Kaffrell, J. Kvasil, G. Løvhøiden, H. Mach, A. Mackova, T. Martinez, G. Nyman, B. Rubio, J. L. Tain, O. Tengblad, T. F. Thorsteinsen, and ISOLDE Collaboration, Nucl. Phys. **A703**, 45 (2002).
[16] V. Barci, G. Ardisson, G. Barci-Funel, B. Weiss, O. El Samad, and R. K. Sheline, Phys. Rev. C **68**, 034329 (2003).
[17] H. Ton, S. Roodbergen, J. Brasz, and J. Blok, Nucl. Phys. **A155**, 245 (1970).
[18] H. Mach, R. L. Gil, and M. Moszyński, Nucl. Instrum. Methods A **280**, 49 (1989).
[19] M. Moszyński and H. Mach, Nucl. Instrum. Methods A **277**, 407 (1989).

[20] H. Mach, F. K. Wohn, G. Molnár, K. Sistemich, J. C. Hill, M. Moszyński, R. L. Gill, W. Krips, and D. S. Brenner, Nucl. Phys. **A523**, 197 (1991).
[21] I. M. Band, M. B. Trzhaskovskaya, C. W. Nestor, P. O. Tikkanen, and S. Raman, At. Data Nucl. Data Tables **81**, 1 (2002).
[22] F. Rösel, H. M. Fries, K. Alder, and H. C. Pauli, At. Data Nucl. Data Tables **21**, 291 (1978).
[23] R. B. Firestone, S. Y. F. Chu, and C. M. Baglin, Table of Isotopes CD-ROM, 8th ed. (Wiley-Interscience, New York, 1999).
[24] A. J. Aas, H. Mach, J. Kvasil, M. J. G. Borge, B. Fogelberg, I. S. Grant, K. Gulda, E. Hagebø, P. Hoff, W. Kurcewicz, A. Lindroth, G. Løvhøiden, A. Mackova, T. Martínez, B. Rubio, M. Sánchez-Vega, J. F. Smith, J. L. Taín, R. B. E. Taylor, O. Tengblad, T. F. Thorsteinsen, and ISOLDE Collaboration, Nucl. Phys. **A654**, 499 (1999).
[25] S. Ćwiok and W. Nazarewicz, Phys. Lett. **B224**, 5 (1989).
[26] S. Ćwiok and W. Nazarewicz, Nucl. Phys. **A529**, 95 (1991).
[27] Y. A. Akovali, Nucl. Data Sheets **58**, 555 (1989).
[28] G. A. Leander and Y. S. Chen, Phys. Rev. C **37**, 2744 (1988).
[29] A. Bohr and B. R. Mottelson, *Nuclear Structure* (Benjamin, Massachusetts, 1975), Vol. 2.
[30] G. Alaga, K. Alder, A. Bohr, and B. R. Mottelson, Mat. Fys. Medd. Dan. Vid. Selsk. **29**, 9 (1955).
[31] V. M. Mikhailov, Izv. Akad. Nauk SSSR, Ser. Fiz. **30**, 1334 (1966).
[32] P. A. Butler and W. Nazarewicz, Rev. Mod. Phys. **68**, 349 (1996).
[33] A. J. Aas, H. Mach, M. J. G. Borge, B. Fogelberg, I. S. Grant, K. Gulda, E. Hagebø, W. Kurcewicz, J. Kvasil, A. Lindroth, T. Martinez, D. Nosek, B. Rubio, J. F. Smith, K. Steffensen, J. L. Taín, O. Tengblad, T. F. Thorsteinsen, and ISOLDE Collaboration, Nucl. Phys. **A611**, 281 (1996).
[34] B. Ackermann, H. Baltzer, C. Ensel, K. Freitag, V. Grafen, C. Günther, P. Herzog, J. Manns, M. Marten-Tölle, U. Müller, J. Prinz, I. Romanski, R. Tölle, J. de Boer, N. Gollwitzer, and H. J. Maier, Nucl. Phys. **A559**, 61 (1993).
[35] S. Raman, C. W. Nestor Jr., and P. Tikkanen, At. Data Nucl. Data Tables **78**, 1 (2001).
[36] M. Dahlinger, E. Kankeleit, D. Habs, D. Schwalm, B. Schwartz, R. S. Simon, J. D. Burrows, and P. A. Butler, Nucl. Phys. **A484**, 337 (1988).
[37] J. R. Hughes, R. Tölle, J. de Boer, P. A. Butler, C. Günther, V. Grafen, N. Gollwitzer, V. E. Holliday, G. D. Jones, C. Lauterbach, M. Marten-Tölle, S. M. Mullins, R. J. Poynter, R. S. Simon, N. Singh, R. J. Tanner, R. Wadsworth, D. L. Watson, and C. A. White, Nucl. Phys. **A512**, 275 (1990).
[38] N. J. Hammond, G. D. Jones, P. A. Butler, R. D. Humphreys, P. T. Greenlees, P. M. Jones, R. Julin, S. Juutinen, A. Keenan, H. Kettunen, P. Kuusiniemi, M. Leino, M. Muikku, P. Nieminen, P. Rahkila, J. Uusitalo, and S. V. Khlebnikov, Phys. Rev. C **65**, 064315 (2002).
[39] J. Kvasil, T. I. Kraciková, M. Finger, and B. Choriev, Czech. J. Phys. B **31**, 1376 (1981); J. Kvasil, T. I. Kraciková, S. Davaa, M. Finger, and B. Choriev, *ibid*. **33**, 626 (1983); T. I. Kraciková, J. Kvasil, S. Davaa, and M. Finger, *ibid.* **35**, 1084 (1985); **36**, 581 (1986).
[40] V. G. Soloviev, *Theory of Complex Nuclei* (Pergamon Press, Oxford, 1976).
[41] A. I. Levon, J. de Boer, G. Graw, J. Kvasil, M. Loewe, V. D. Valnion, M. Würkner, H. Baltzer, C. Günther, J. Manns, U. Müller, and T. Weber, Nucl. Phys. **A598**, 11 (1996).
[42] P. Kálmán and T. Bükki, Phys. Rev. C **63**, 027601 (2001).
[43] T. Mitsugashira, M. Hara, T. Ohtsuki, H. Yuki, K. Takamiya, Y. Kasamtsu, A. Shinohara, H. Kikunaga, and T. Nakanishi, J. Radioanal. Nucl. Chem. **255**, 63 (2003).
[44] P. Möller and J. R. Nix, At. Data Nucl. Data Tables **39**, 213 (1988).
[45] J. Dudek, Z. Szymański, and T. Werner, Phys. Rev. C **23**, 920 (1981).